Dynamical and elastic properties of MgSiO 3 perovskite (bridgmanite)

Björn Wehinger, Alexeï Bosak, Sabrina Nazzareni, Daniele Antonangeli, Alessandro Mirone, Samrath Lal Chaplot, Ranjan Mittal, Eiji Ohtani, Anton Shatskiy, Surendra Saxena, et al.

AGU PUBLICATIONS

Geophysical Research Letters

RESEARCH LETTER
10.1002/2016GL067970

Key Points:
- Lattice dynamics of $MgSiO_3$-bridgmanite
- Phonon spectroscopy by inelastic X-ray scattering
- Lattice dynamics by density functional perturbation theory

Supporting Information:
- Supporting Information S1
- Data Set 1
- Data Set 2
- Data Set 3

Correspondence to:
B. Wehinger,
bjorn.wehinger@unige.ch

Citation:
Wehinger, B., et al. (2016), Dynamical and elastic properties of $MgSiO_3$ perovskite (bridgmanite), *Geophys. Res. Lett.*, *43*, 2568–2575, doi:10.1002/2016GL067970.

Received 26 JAN 2016
Accepted 2 MAR 2016
Accepted article online 8 MAR 2016
Published online 29 MAR 2016

Dynamical and elastic properties of $MgSiO_3$ perovskite (bridgmanite)

Björn Wehinger[1,2], Alexeï Bosak[3], Sabrina Nazzareni[4], Daniele Antonangeli[5], Alessandro Mirone[3], Samrath Lal Chaplot[6], Ranjan Mittal[6], Eiji Ohtani[7], Anton Shatskiy[8,9], Surendra Saxena[10], Subrata Ghose[11,12], and Michael Krisch[3]

[1]Department of Quantum Matter Physics, University of Geneva, Geneva, Switzerland, [2]Laboratory for Neutron Scattering and Imaging, Paul Scherrer Institute, Villigen, Switzerland, [3]European Synchrotron Radiation Facility, Grenoble, France, [4]Department of Physics and Geology, University of Perugia, Perugia, Italy, [5]Institut de Minéralogie, de Physique des Matériaux, et de Cosmochimie (IMPMC), UMR CNRS 7590, Sorbonne Universités – UPMC, Muséum National d'Histoire Naturelle, Paris, France, [6]Solid State Physics Division, Bhabha Atomic Research Centre, Bombay, India, [7]Department of Earth Science, Graduate School of Science, Tohoku University, Sendai, Japan, [8]V.S. Sobolev Institute of Geology and Mineralogy, Siberian Branch, Russian Academy of Sciences, Novosibirsk, Russia, [9]Department of Geology and Geophysics, Novosibirsk State University, Novosibirsk, Russia, [10]Center for the Study of Matter at Extreme Conditions, Florida International University, Miami, USA, [11]Department of Earth and Space Sciences, University of Washington, Seattle, Washington, USA, [12]Deceased 21 January 2015

Abstract We report on the lattice dynamics of $MgSiO_3$ perovskite (bridgmanite). Phonon spectroscopy was performed employing inelastic X-ray scattering from single crystals, and the results were confronted to ab initio calculations. We observe a remarkable agreement between experiment and theory, and provide accurate results for phonon dispersion relations, the vibrational density of states, and the full elasticity tensor. The present work constitutes an important milestone fully validating the lattice dynamics calculation against precise experimental evidence and marks a starting point to extend this kind of combined studies to the high-pressure and high-temperature conditions directly relevant for the physical properties and chemical composition of Earth's lower mantle.

1. Introduction

The Earth's lower mantle extends from 670 to 2900 km in depth and represents roughly 60% of Earth's total volume. Numerous studies indicate that compositionally the lower mantle consists of magnesium silicate with Fe and Al as minor elements [*Andrault et al.*, 2001; *Hummer and Fei*, 2012; *Murakami et al.*, 2012]. Phase equilibrium experiments and calculations have established that forsterite (Mg_2SiO_4) and stishovite (SiO_2) react to form $MgSiO_3$ perovskite at about 24 GPa; the perovskite continues down to about 110 GPa when it transforms to a postperovskite phase [*Fabrichnaya et al.*, 2004; *Oganov and Price*, 2005]. Accordingly, magnesium perovskite is to be considered as the volumetrically most abundant mineral on the Earth. However, irrespectively of its abundance, the natural occurrence of $MgSiO_3$ perovskite was reported only very recently [*Tschauner et al.*, 2014], in the Tenham L6 chondrite, a shocked meteorite, as the mineral is metastable under ambient condition and unpreservable during the exhumation of terrestrial mantle rocks. After the discovery, $MgSiO_3$ has been named bridgmanite [*Tschauner et al.*, 2014].

The determination of the physical properties of bridgmanite is of fundamental geophysical interest. Indeed, while the analysis of seismic records allows the determination of compressional and shear velocities in situ, the establishment of a compositional and mineralogical model for the mantle requires the knowledge of the mineral's equation of state and its elastic and thermodynamic properties at the relevant conditions of pressure and temperature. Structural studies at such extreme conditions have been extensively performed by X-ray diffraction on samples compressed in laser-heated diamond anvil cells [e.g., *Fiquet et al.*, 1998, 2000; *Boffa Ballaran et al.*, 2012] and provide important insight into the pressure-volume relationship and its dependence on temperature. However, sound velocities as well as other key thermodynamic quantities of primary geophysical importance, such as heat capacity, entropy, and enthalpy, necessary for the interpretation of the preliminary reference Earth model and seismic tomography and to produce convection and mantle adiabatic models, are dynamical properties, which so far have been largely derived by calculations. Thus, the full knowledge of the phonon dispersion and the validation of the eigenvectors are required to substantiate the currently untested accuracy of lattice dynamics calculations and the derived thermodynamic

and elastic properties. The elasticity tensor of $MgSiO_3$ perovskite at ambient conditions has been determined from measurements on both single-crystal and polycrystalline samples [*Yeganeh-Haeri*, 1994; *Sinogeikin et al*., 2004]. The aggregate shear modulus has been measured up to 96 GPa [*Murakami et al*., 2007]. Numerous ab initio calculations have been performed as well, with the aim not only to reproduce the experimental structural studies but also to predict thermodynamic and elastic properties, phase stability, and effects of anharmonicity via the calculation of the phonon dispersion [*Parlinski and Kawazoe*, 2000; *Karki et al*., 2000; *Wentzcovitch et al*., 2004; *Oganov and Price*, 2005; *Carrier et al*., 2007; *Zhang et al*., 2014]. Noteworthy, despite this large body of theoretical calculations, there is not a single experimental phonon dispersion study. This is largely explained by the fact that single crystals of sufficiently good quality are only available in very small quantities. This excludes the utilization of inelastic neutron scattering measurements, but it presents a unique opportunity for inelastic X-ray scattering (IXS) with meV energy resolution. IXS experiments can be performed in diamond anvil cells (DACs), thus enabling combined pressure-temperature studies at Mbar pressure and temperatures up to 1100 K [*Fiquet et al*., 2004; *Krisch and Sette*, 2007; *Ghose et al*., 2006; *Antonangeli et al*., 2011, 2012].

In the present work we utilize IXS to measure the phonon dispersion of single crystal $MgSiO_3$ along the main symmetry directions at ambient conditions. The experimental results are confronted with lattice dynamics calculations from first principles. Excitation spectra are directly compared with computed scattering intensities, which allow the validation of both calculated eigenvalues and eigenvectors. We benchmark our results by comparing the derived elastic moduli with Brillouin light scattering measurements and the energies of Raman active modes with experimental values available in literature.

2. Experimental Details

The bridgmanite crystals were synthesized starting from 85 mol % $MgSiO_3$ (enstatite) + 15 mol % Mg_2SiO_4 (forsterite) mixture as a silicate source. H_2O was used as a solvent, and the bulk water content of the sample was about 13 wt %. Synthesis conditions were $P = 24$ GPa and $T = 1500$°C, with heating duration of 20 min using a Kawai type 5000 ton multianvil press at Okayama University. Details of the synthesis procedure of bridgmanite can be found elsewhere [*Shatskiy et al*., 2007]. The water content is estimated to be about 140 (52) wt ppm using polarized IR spectra of thin sections perpendicular to *a*, *b*, and *c* axes of bridgemanite.

Optically transparent samples were characterized by single-crystal X-ray diffraction using an Xcalibur diffractometer (Rigaku-Oxford Diffraction) using Mo $K\alpha$ radiation (Mo $K\alpha_1$ 0.70936 Å and Mo $K\alpha_2$ 0.71359 Å) and a CCD detector. Most of the samples proved to be twins, except one. Diffraction data were collected on this sample ($50 \times 50 \times 100$ μm in size) via omega scans (66.57 mm detector-to-sample distance, 25 s per frame, 1° frame width) up to 37° in Bragg theta angle. The crystal structure of $MgSiO_3$ bridgmanite, orthorhombic, *Pnma*, consists of corner-linked SiO_6 octahedra with Mg in an irregular tenfold coordination. We determined lattice constants $a = 4.9436(3)$ Å, $b = 6.9149(8)$ Å, and $c = 4.7902(6)$ Å. Data collected were merged obtaining a discrepancy factor among symmetry related reflections (internal discrepancy factor $R_{int} = 3.1\%$), and typical rocking curve widths were of about 0.4°. The structure was refined using SHELXL program [*Sheldrick*, 2008] in the space group *Pnma*. Anisotropic refinement cycles converged to a discrepancy factor $R_1 = 2.5\%$ for $535 Fo > 4\sigma Fo$ and a goodness of fit of 1.106. Bonds and angles are similar to literature data [*Yagi et al*., 1978].

Phonon spectroscopy measurements were conducted at the Inelastic X-ray Scattering Beamline ID28 of the European Synchrotron Radiation Facility, in Grenoble (France). We have used the Si (9 9 9) reflection for both main monochromator and analyzer crystals, which provides an incident energy of 17,794 keV and 3 meV overall instrumental resolution. A focusing optic with a multilayer mirror allowed a spot size of 30 (horizontal) by 80 (vertical) μm^2 full width at half maximum (FWHM) at the sample position. Scattering angle and sample orientation determined the momentum transfer *Q* (direction and size). The momentum resolution was defined by slits in front of the analyzers and set to 0.28 nm^{-1} and 0.84 nm^{-1} in the horizontal and vertical scattering plane, respectively. A detailed description of the experimental setup can be found elsewhere [*Krisch and Sette*, 2007].

3. Lattice Dynamics Calculations

First principle calculations were carried out utilizing the generalized gradient approximation (GGA) to the density functional theory in Perdew-Burke-Ernzerhof (PBE) parameterization as implemented in the CASTEP

code [*Clark et al.*, 2005]. GGA was preferred over the local density approximation (LDA) because of the large polarizability in $MgSiO_3$. Born effective charges and dielectric properties are rather well described in PBE parameterization [*Refson et al.*, 2006], and these properties are required to correctly treat the splitting of longitudinal optical and transverse optical modes. The pseudopotentials were of the norm-conserving type and created using the optimized method of *Rappe et al.* [1990] with single projectors. The pseudopotentials explicitly include three reference orbitals as valence states for magnesium and silicon and two for oxygen. Wave functions were expanded in a plane wave basis set, truncated at a kinetic cutoff energy of 800 eV and sampled at special k points on a $4\times3\times4$ Monkhorst Pack grid. The obtained convergence for internal forces was below 10^{-4} eV/Å. The structure was fully relaxed in the Broyden-Fletcher-Goldfarb-Shannon scheme by varying both internal coordinates and lattice parameters [*Pfrommer et al.*, 1997]. The calculated lattice constants at zero temperature agree within 1.1% with the experimental values at 77 K (values are given in Table S1 in the supporting information). The dynamical matrices were computed on a $5\times3\times5$ Monkhorst Pack grid employing density functional perturbation theory [*Refson et al.*, 2006; *Gonze et al.*, 1994]. Phonon energies and eigenvectors at arbitrary momentum transfer were calculated by Fourier interpolation in the cumulate scheme, which includes all image force constants [*Parlinski et al.*, 1997]. Phonon energies were converged to a level of <0.1 meV. We imposed sum rule corrections for acoustic phonons and Born effective charges with maximal correction of 3 meV at Γ. For the calculation of IXS intensities we assumed both adiabatic and harmonic approximations to be valid. The calculation includes Debye-Waller factors derived from dynamical matrices on a fine grid and Q-dependent scattering factors [*Krisch and Sette*, 2007; *Wehinger et al.*, 2014]. Thermodynamic properties are evaluated within the quasi-harmonic approximation.

The elasticity tensor was calculated using a least squares fit as detailed below. A sphere in reciprocal space containing 485 q points close to Γ with $|q|\leq0.02$ relative lattice units was used for this fit, and the dynamical matrices on these q points were computed using Fourier interpolation. According to the definition of acoustic phonons, the deformation energies can be calculated at each q point, using the dynamical matrix and the same displacement modulus and polarization for all atomic sites. A given choice of displacement and q vector determine the deformation tensor. In elasticity theory, the deformation energy can be expressed as a linear combination of the elastic constants for the given deformation tensor. We impose via a least squares fit that the two ways of calculating the deformation energy coincide for all the considered q points and polarizations and obtain in this way the elasticity tensor.

4. Results

Figure 1 illustrates representative IXS spectra at selected reduced momentum transfers as specified in the legends and figure caption. The experimental spectra show an elastic line, which is centered at zero energy transfer, and several inelastic features between 20 and 110 meV, corresponding to acoustic and optical phonons. A logarithmic intensity scale is chosen for better visualization of the high-energy phonon modes, which have much weaker intensities. Solid blue lines in the individual panels represent the calculated inelastic contribution. The computed energy transfer scale was adjusted by a single factor of 1.05, and for each Q value, the intensities were also scaled by a single factor to obtain best agreement with the experimental results. The contribution at zero energy transfer, due to elastic and quasi-elastic diffuse scattering, is observed in the experiments but is not accounted for by the calculation.

Figure 2 compares experimental and theoretical IXS intensity maps along three selected principal directions in reciprocal space. These give a more global overview on the complex phonon dispersion and the intensity evolution as a function of momentum transfer Q. Besides a strong contribution from the elastic line close to the (0 4 0) point and some artifacts due to the interpolation routine used for the reconstruction of the IXS maps from individual fixed-Q IXS experimental spectra, we note a very good overall agreement both in phonon energies and intensities. Together with the results displayed in Figure 1 this proves that our calculations correctly predict not only the phonon energies (after a modest overall scaling) but also the phonon eigenvectors, which govern the intensities [*Bosak et al.*, 2009]. This is an unprecedented validation of the theoretical treatment. The slight but systematic underestimation of the phonon energies is expected and is due to a small inaccuracy in the exchange correlation functional (see *Refson et al.* [2006] for a detailed discussion).

In Figure 3 we display the $MgSiO_3$ phonon dispersion along selected high-symmetry directions. For the low-energy part we superimpose the experimentally determined phonon energies. These were obtained by

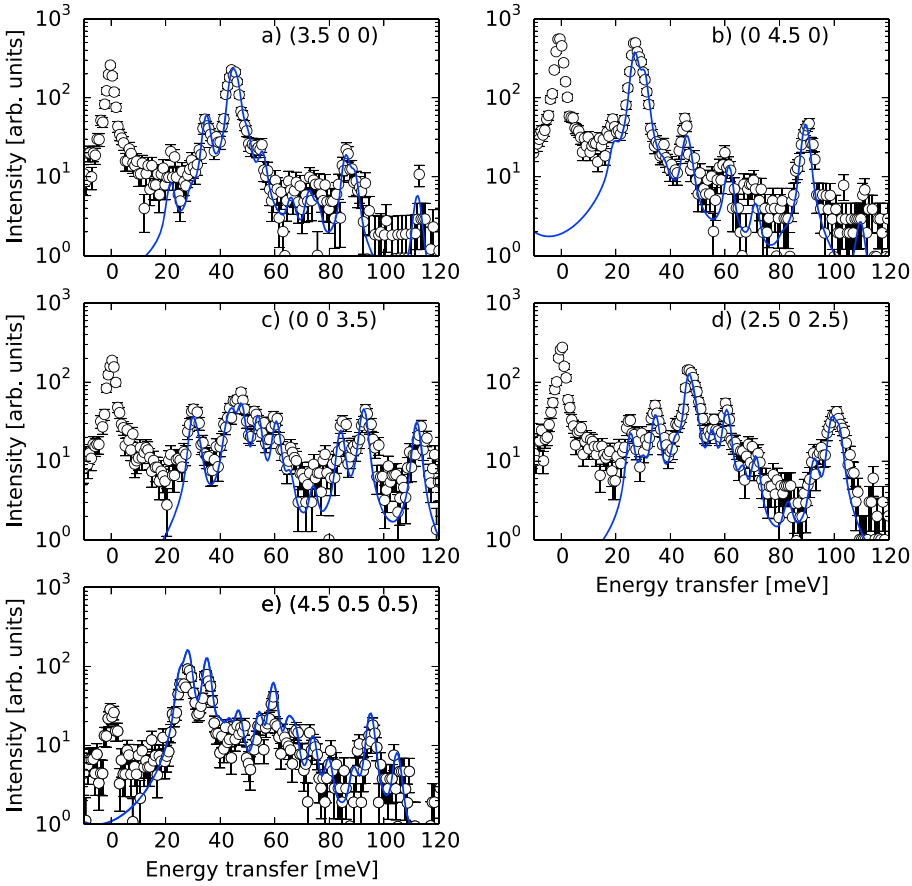

Figure 1. Single-crystal IXS spectra of $MgSiO_3$ as obtained from experiment (open symbols with corresponding error bars) and calculation (blue lines) at reciprocal space points (a) *X*, (b) *Y*, (c) Z, (d) *U*, and (e) *R*. The ab initio calculated phonon energies were multiplied by 1.05, and the intensities were convoluted with the instrumental response.

a least square fit of Lorentzian functions to the IXS spectra. The excitations were herby convoluted with the experimental instrument response. The agreement with the calculation is excellent. Inspection of the complete phonon dispersion—which extends up to 120 meV—reveals that the correct assignment of an experimentally observed phonon mode becomes increasingly more difficult due to the high density of phonon branches. Nonetheless, the already mentioned remarkable agreement between experiment and theory (after a mere rescaling) makes us confident that the calculation correctly describes the full lattice dynamics of $MgSiO_3$. The phonon dispersion of the optical branches is rather complex and shows pronounced splitting of longitudinal optical and transverse optical branches. The splitting is due to large Born effective charges and the symmetry of the system. $MgSiO_3$ exhibits 24 Raman active modes of which 14 have been determined by experiments [*Gillet et al.*, 2000]. The calculated energies are given and compared to experiments in Table S2. Values were assigned by carefully comparing calculated and measured intensities. The mode at 99.3 meV should be visible in experiment but is beyond the measured energy transfers of the reported measurements. We observe a very good agreement between experiment and calculation with the only exception of the mode with a calculated energy of 63.7 meV.

The so-validated theoretical results were used to derive the partial and total phonon density of states (DOS), shown in Figure 4. The partial contributions per species indicate that the vibration of oxygen atoms dominates the first two low-energy peaks in the DOS. Between 67 and 82 meV all modes are almost exclusively due to oxygen, which enables species-specific spectroscopy. We further note a gap between 100 and 102 meV. The total DOS is in good agreement with the previous DFPT calculation using the LDA [*Karki et al.*, 2000]. Distinct features like the position of the first two low-energy peaks and the gap are located at very similar energies and show the same intensity ratios. We stress that our DOS is more detailed

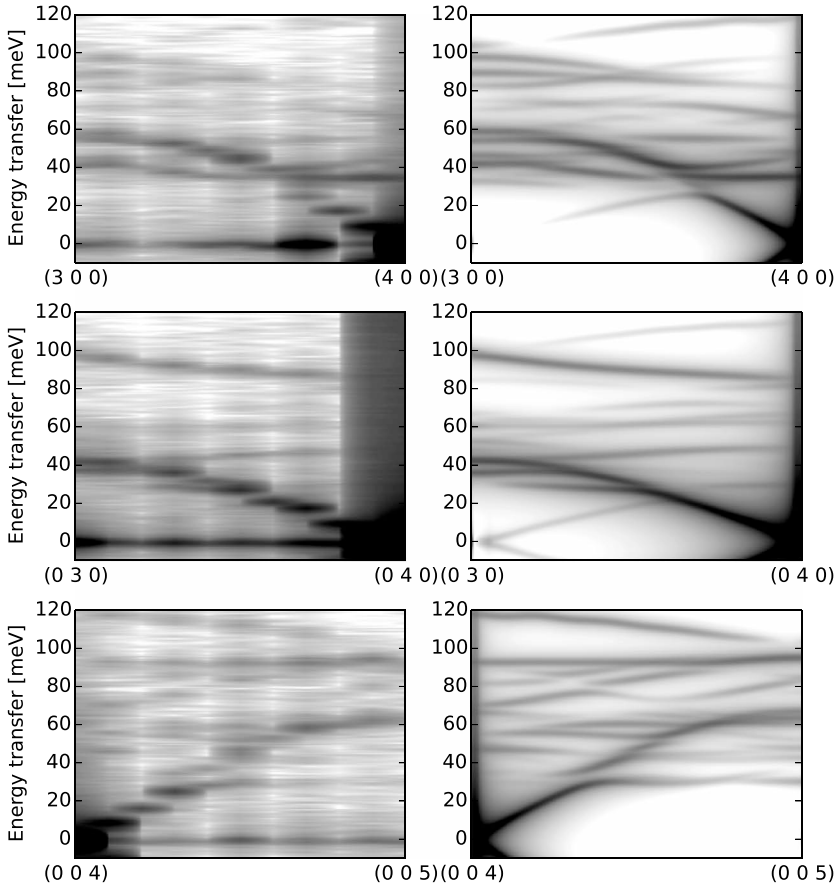

Figure 2. IXS intensity maps from (left column) experiment and (right column) calculation along selected directions in reciprocal space on a logarithmic intensity scale. Each experimental map consists of the linear interpolation of eleven spectra. The calculated intensities were obtained from 200 *q* points along each direction. Phonon energies were multiplied by 1.05 and the excitations convoluted with the instrumental response.

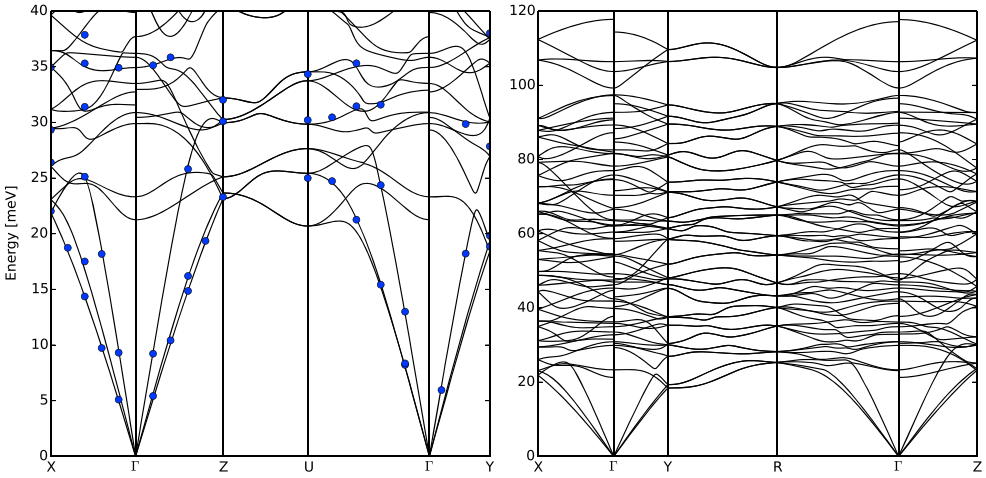

Figure 3. Calculated phonon dispersion (solid lines) along high-symmetry directions. (left) A zoom of the low-energy part; (right) the full energy range. Experimentally determined phonon energies are plotted as blue dots, the calculated energies are scaled by 1.05.

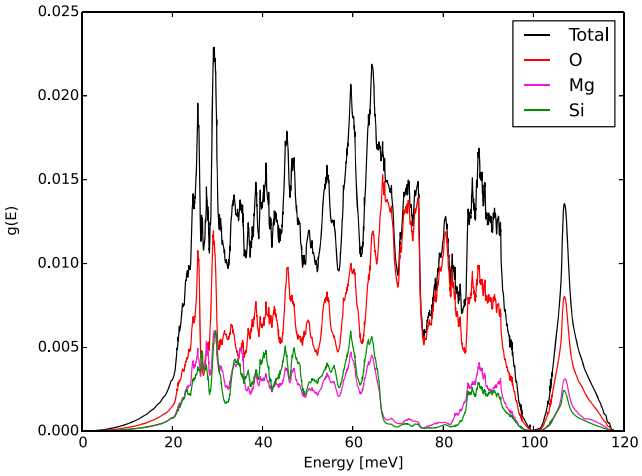

Figure 4. Calculated vibrational density of states of $MgSiO_3$ (solid black line). The partial contribution per species is highlighted by the use of different colors. The energy is scaled by 1.05.

due to a very dense q grid. The total DOS allows the derivation of important thermodynamic properties via integral equations [*Jones and March*, 1973]. Some relevant thermodynamic quantities calculated within the quasi-harmonic approximation for room temperatures can be found in the supporting information (see Table S3).

The full elasticity tensor is given in Table 1. The elastic moduli were determined using a least squares fit to acoustic phonons without the need of symmetry braking displacements. The energy scaling was not applied here, because the elasticity and the acoustic phonons very close to Γ are correctly described by the employed calculation. This can be readily judged by the very good agreement between the resulting bulk modulus (247 GPa) with results from LDA calculations (247 GPa in *Karki et al.* [2000]) and experimental values (253 and 264 GPa in *Sinogeikin et al.* [2004] and *Yeganeh-Haeri* [1994], respectively). The bulk modulus presented here is higher than the value reported from previous calculations using GGA (231 GPa in *Oganov et al.* [2001]). This difference can mainly be attributed to the fact that our value has been derived from the acoustic phonons energies rather than from the stress-strain relation. The applied method provides a useful tool to derive the elasticity tensor directly from the lattice dynamics. It profits from the acoustic sum rule corrections, which overcome numerical issues due to the finite grid sampling of reciprocal space and finite number of plane waves. As further advantage, in contrast to stress-strain calculations using distorted structures, all structural symmetry operations can be exploited to reduce the number of k points used for sampling the Brillouin zone. The calculations are thus much easier to converge. Within our approach, results of IXS measurements have been used to validate the acoustic phonons calculations. Direct determination of the full elasticity tensor via IXS would require measurements with additional sample orientations. For completeness we also employed the traditional method exploiting the stress-strain relation from 18 distorted structures, which leads to values comparable to previous calculations using GGA [*Oganov et al.*, 2001] and a resulting bulk modulus of 232 GPa. The calculated elastic constants agree well with literature values determined by Brillouin light scattering (BLS) [*Sinogeikin et al.*, 2004; *Yeganeh-Haeri*, 1994].

Considering the independent elements of the elastic tensor, we note that $C_{11} > C_{33} > C_{22}$, which implies an anisotropic compressional behavior for $MgSiO_3$ bridgmanite with the b axis (c axis in the *Pbnm* space group) the most compressible and the a axis the least compressible (b axis in the *Pbnm* space group).

Table 1. Elastic Moduli in GPa Derived From the Present Ab Initio Calculations, by Fitting the Elasticity Tensor to Acoustic Phonons at Low q (DFPT)[a]

	C_{11}	C_{22}	C_{33}	C_{44}	C_{55}	C_{66}	C_{12}	C_{13}	C_{23}
DFPT	511(2)	426(2)	494(2)	176(1)	151(1)	193(1)	149(1)	109(1)	137(1)
BLS1	528	456	481	182	147	200	146	125	139
BLS2	537	485	482	186	147	204	146	144	147
DFT	488	412	440	158	133	183	135	114	123
DFT1	489	408	444	172	131	194	136	110	126
DFT2	500	434	449	162	138	183	144	123	129

[a]Experimental values are reported for comparison from BLS [*Sinogeikin et al.*, 2004; *Yeganeh-Haeri*, 1994], BLS1, and BLS2, respectively, and calculated values via stress-strain relation using GGA (our study: DFT, *Oganov et al.* [2001]: DFT1) and using LDA [*Wentzcovitch et al.*, 2004] (DFT2).

From the elastic moduli, beside the already discussed bulk modulus, we can also calculate the Voigt-Reuss-Hill average values for the shear modulus G, the Young modulus E, the Poisson ratio ν, and the aggregate velocities, longitudinal (or compressional) v_p, and shear v_s (see Table S4). The geophysical parameters which we obtain from the Reuss-Voigt-Hill approximation agree better with experimental values than previous ab initio calculations (see Table S4). This further strengthens the importance of the experimental validation of the lattice dynamics calculation.

5. Summary and Perspectives

Our experimental study combined with parameter-free calculations provides a complete picture of the lattice dynamics in $MgSiO_3$ brigmanite, the principal mineral phase of the Earth's lower mantle. Its lattice dynamics contains many subtle features like a pronounced splitting of longitudinal and transverse optical modes and strongly dispersive optical branches, which make the detailed knowledge of the full phonon dispersion crucial for validating any physical quantity related to the lattice dynamics. Our results unequivocally substantiate the aptness of the employed calculation and show the range of validity for the computational approaches used in geophysical models. The comparison of the DOS and elastic constants with results from previous calculations using LDA and GGA shows that both approximations correctly describe the elastic and thermodynamic properties of $MgSiO_3$ brigmanite at ambient pressure and temperature conditions. We are thus confident that geophysical models based on such kind of calculations can provide accurate predictions for values at mantle relevant conditions within the limits given by the extension of the calculation to high pressures and temperatures. Moreover, our work clearly demonstrates that the phonon related properties of many geophysically relevant materials can be obtained without the need to record the phonon branches one by one along all high-symmetry directions. We have shown that the determination of a representative subset of experimental data is sufficient for the reliable determination of the full lattice dynamics. This is not a trivial gain for low-symmetry minerals. Consequently, very important thermodynamic and elastic properties can be derived with high accuracy. Furthermore, when extended to high-pressure and high-temperature conditions, it allows the validation of the phase stability proposed on the basis of energy minimization. It is worth noting that the availability of a single crystal, while beneficial, is not mandatory, and the very same concept can be applied to polycrystalline materials as was demonstrated in the case of stishovite [*Bosak et al*., 2009].

The here-reported study at ambient conditions marks the starting point for a comprehensive investigation of the stable phases in Earth's mantle, including Mg_2SiO_4 (forsterite, spinel, and β-phase), $MgSiO_3$ (orthopyroxene, ilmenite, and perovskite), and SiO_2 (stishovite and seifertite) at pressures and temperatures relevant for the Earth's lower mantle. The possibility offered at ID28 to focus the X-ray beam down to $17 \times 10\ \mu m^2$ with a flux reduction of only ~25–30% compared to the optical configuration used in the present experiment ensures the feasibility of such kind of study. Indeed, experiments can be efficiently performed on samples as small as few tens of microns in size. Samples as thin as 15–20 μm may be used in a diamond anvil cell (DAC) up to Mbar pressures.

Acknowledgments
We are grateful to Artem Oganov and Guangrui Qian for the preliminary phonon calculations. Beamtime was granted on beamline ID28 at the ESRF in the frame of proposal HS-4807. The data are available from the figures and tables of this letter and the supporting information. A. Shatskiy acknowledges the support from Ministry of Education and Science of Russian Federation (No 14.B25.31.0032). This paper is devoted to Subrata Ghose, a friend and colleague. He was a visionary mineralogist and a great man.

References

Akaogi, M., and E. Ito (1993), Refinement of enthalpy measurement of $MgSiO_3$ perovskite and negative pressure-temperature slopes for Perovskite-forming reactions, *Geophys. Res. Lett.*, *20*, 1839–1842, doi:10.1029/93GL01265.

Andrault, D., N. Bolfan-Casanova, and N. Guignot (2001), Equation of state of lower mantle (Al,Fe)-$MgSiO_3$ perovskite, *Earth Planet. Sci. Lett.*, *193*, 501–508.

Antonangeli, D., J. Siebert, C. M. Aracne, D. L. Farber, A. Bosak, M. Hoesch, M. Krisch, F. J. Ryerson, G. Fiquet, and J. Badro (2011), Spin crossover in ferropericlase at high pressure: A seismologically transparent transition?, *Science*, *331*, 64.

Antonangeli, D., T. Komabayashi, F. Occelli, E. Borissenko, A. C. Walters, G. Fiquet, and Y. Fei (2012), Simultaneous sound velocity and density measurements of hcp iron up to 93 GPa and 1100 K: An experimental test of the Birch's law at high temperature, *Earth Planet. Sci. Lett.*, *331–332*, 210–214.

Boffa Ballaran, T., A. Kurnosov, K. Glazyrin, D. Frost, M. Merlini, M. Hanfland, and R. Caracas (2012), Effect of chemistry on the compressibility of silicate perovskite in the lower mantle, *Earth Planet. Sci. Lett.*, *333–334*, 181–190.

Bosak, A., I. Fischer, M. Krisch, V. Brazhkin, T. Dyuzheva, B. Winkler, D. Wilson, D. Weidner, K. Refson, and V. Milman (2009), Lattice dynamics of stishovite from powder inelastic X-ray scattering, *Geophys. Res. Lett.*, *36*, L19309, doi:10.1029/2009GL040257.

Carrier, P., R. Wentzcovitch, and J. Tsuchiya (2007), First principles prediction of crystal structures at high temperatures using the quasiharmonic approximation, *Phys. Rev. B*, *76*(6), 064116.

Clark, S., M. Segall, C. Pickard, P. Hasnip, M. Probert, K. Refson, and M. Payne (2005), First principles methods using CASTEP, *Z. Kristallogr.*, *220*, 567–570.

Fabrichnaya, O., S. K. Saxena, P. Richet, and E. F. Westrum (2004), *Thermodynamic Data, Models and Phase Diagrams in Multicomponent Oxide Systems*, Springer, Berlin.

Fiquet, G., D. Andrault, A. Dewaele, T. Charpin, M. Kunz, and D. Hausermann (1998), P-V-T equation of state of $MgSiO_3$ perovskite, *Phys. Earth Planet. Inter.*, *105*, 21–31.

Fiquet, G., A. Dewaele, D. Andrault, M. Kunz, and M. Le Bihan (2000), Thermoelastic properties and crystal structure of $MgSiO_3$ perovskite at lower mantle pressure and temperature conditions, *Geophys. Res. Lett.*, *27*, 21–24, doi:10.1029/1999GL008397.

Fiquet, G., J. Badro, F. Guyot, C. Bellin, M. Krisch, D. Antonangeli, A. Mermet, H. Requardt, D. Farber, and J. Zhang (2004), Application of inelastic X-ray scattering to measurements of acoustic wave velocities in geophysical materials at very high pressure, *Phys. Earth Planet. Inter.*, *143–144*, 5–18.

Ghose, S., M. Krisch, A. R. Oganov, A. Beraud, A. Bosak, R. Gulve, R. Seelaboyina, H. Yang, and S. K. Saxena (2006), Lattice dynamics of MgO at high pressure: Theory and experiment, *Phys. Rev. Lett.*, *96*, 035507.

Gillet, P., I. Daniel, F. Guyot, J. Matas, and J. C. Chervin (2000), A thermodynamic model for $MgSiO_3$-perovskite derived from pressure, temperature and volume dependences of the Raman mode frequencies, *Phys. Earth Planet. Inter.*, *117*, 361–384.

Gonze, X., J. Charlier, D. Allan, and M. Teter (1994), Interatomic force constants from first principles: The case of α-quartz, *Phys. Rev. B*, *50*, 13,035.

Hummer, D. R., and Y. Fei (2012), Synthesis and crystal chemistry of Fe^{3+}-bearing $(Mg,Fe^{3+})(Si,Fe^{3+})O_3$ perovskite, *Am. Mineral.*, *97*, 1915–1921.

Jones, W., and N. H. March (1973), *Theoretical Solid State Physics*, John Wiley, London.

Karki, B. B., R. M. Wentzcovitch, S. de Gironcoli, and S. Baroni (2000), Ab initio lattice dynamics of $MgSiO_3$ perovskite at high pressure, *Phys. Rev. B*, *62*, 14,750–14,756.

Krisch, M., and F. Sette (2007), Inelastic X-ray scattering from phonons, in *Light Scattering in Solids, Novel Materials and Techniques*, *Top. Appl. Phys.*, vol. 108, pp. 317–370, Springer, Berlin.

Murakami, M., S. V. Sinogeikin, H. Hellwig, J. D. Bass, and J. Li (2007), Sound velocity of $MgSiO_3$ perovskite to Mbar pressure, *Earth Planet. Sci. Lett.*, *256*, 47–54.

Murakami, M., Y. Ohishi, N. Hirao, and K. Hirose (2012), A perovskitic lower mantle inferred from high-pressure, high-temperature sound velocity data, *Nature*, *485*, 90–94.

Oganov, A. R., and G. D. Price (2005), Ab initio thermodynamics of $MgSiO_3$ perovskite at high pressures and temperatures, *J. Chem. Phys.*, *122*, 124501.

Oganov, A. R., J. P. Brodholt, and G. D. Price (2001), Ab initio elasticity and thermal equation of state of $MgSiO_3$ perovskite, *Earth Planet. Sci. Lett.*, *184*, 555–560.

Parlinski, K., and Y. Kawazoe (2000), Ab initio study of phonons and structural stabilities of the perovskite-type $MgSiO_3$, *Eur. Phys. J. B*, *16*, 49–58.

Parlinski, K., Z. Li, and Y. Kawazoe (1997), First-principles determination of the soft mode in cubic ZrO_2, *Phys. Rev. Lett.*, *78*, 4063–40,666.

Pfrommer, B., M. Côté, S. Louie, and M. Cohen (1997), Relaxation of crystals with the quasi-Newton method, *J. Comput. Phys.*, *131*, 233–240.

Rappe, A. M., K. M. Rabe, E. Kaxiras, and J. D. Joannopoulos (1990), Optimized pseudopotentials, *Phys. Rev. B*, *41*, 1227.

Refson, K., P. Tulip, and S. Clark (2006), Variational density-functional perturbation theory for dielectrics and lattice dynamics, *Phys. Rev. B*, *73*, 155114.

Ross, N., and R. Hazen (1989), Single crystal X-ray diffraction study of $MgSiO_3$ perovskite from 77 to 400 K, *Phys. Chem. Miner.*, *16*, 415–420.

Shatskiy, A., H. Fukui, T. Matsuzaki, K. Shinoda, A. Yoneda, D. Yamazaki, E. Ito, and T. Katsura (2007), Growth of large (1 mm) $MgSiO_3$ perovskite single crystals: A thermal gradient method at ultrahigh pressure, *Am. Mineral.*, *92*, 1744–1749.

Sheldrick, G. M. (2008), A short history of SHELX, *Acta Crystallogr., Sect. A: Found. Adv.*, *A64*, 112–122.

Sinogeikin, S. V., J. Zhang, and J. D. Bass (2004), Elasticity of single crystal and polycrystalline $MgSiO_3$ perovskite by Brillouin spectroscopy, *Geophys. Res. Lett.*, *31*, L06620, doi:10.1029/2004GL019559.

Tschauner, O., C. Ma, J. R. Beckett, C. Prescher, V. Prapapenka, and G. R. Rossman (2014), Discovery of bridgmanite, the most abundant mineral in Earth, in a shocked meteorite, *Science*, *346*, 6213.

Wehinger, B., A. Bosak, G. Piccolboni, K. Refson, D. Chernyshov, A. Ivanov, A. Rumiantsev, and M. Krisch (2014), Diffuse scattering in metallic tin polymorphs, *J. Phys. Condens. Matter*, *26*, 115401.

Wentzcovitch, R. M., B. B. Karki, M. Cococcioni, and S. de Gironcoli (2004), Thermoelastic properties of $MgSiO_3$-perovskite: Insights on the nature of the Earth's lower mantle, *Phys. Rev. Lett.*, *92*, 018501.

Yagi, T., H.-K. Mao, and P. M. Bell (1978), Structure and crystal chemistry of perovskite-type $MgSiO_3$, *Phys. Chem. Miner.*, *3*, 97–110.

Yeganeh-Haeri, A. (1994), Synthesis and re-investigation of the elastic properties of single-crystal magnesium silicate perovskite, *Phys. Earth Planet. Inter.*, *87*, 111–121.

Zhang, D. B., T. Sun, and R. M. Wentzcovitch (2014), Phonon quasi-particles and anharmonic free energy in complex systems, *Phys. Rev. Lett.*, *112*, 058501.